

# Concepts and Methodologies for Track Improvement and Associated Physical Modelling and Field Monitoring



**Buddhima Indraratna, Ngoc Trung Ngo, Qideng Sun,  
Cholachat Rujikiatkamjorn and Fernanda Bessa Ferreira**

**Abstract** As the heavy haul freight trains become longer and heavier, ballast grain experience pronounced breakage and deformation, resulting in the deterioration of the ballasted track substructure. Suitable soil stabilisation approaches using geosynthetics and/or energy-absorbing rubber mats are commonly employed to enhance the stability and longevity of ballasted tracks. This paper reviews the research studies that have been conducted at the University of Wollongong on track technology using advanced laboratory and computational modelling, as well as real-life health monitoring of selected track sections. Full-scale instrumented field monitoring supported by Australian rail organisations has been carried out to obtain measurements of actual stresses and displacements and thereby evaluate track performance supplemented by computational models. In the past decade, the authors have tested varied types of geosynthetics and rubber mats both in the laboratory and in the field where these geoinclusions were put underneath the ballast layer in tracks built on various subgrade types (i.e. soft and hard subgrades). Stresses induced by traffic, ballast degradation, vertical and lateral displacements of the ballast aggregates were routinely recorded using extensive instrumentation systems. These results provide suitable approaches that can be considered into current track design for future heavy and long freight train travelling at higher speeds.

---

B. Indraratna (✉) · N. T. Ngo · Q. Sun · C. Rujikiatkamjorn · F. B. Ferreira  
Centre for Geomechanics and Railway Engineering (CGRE) and ARC Training  
Centre for Advanced Technologies in Rail Track Infrastructure (ITTC-Rail),  
University of Wollongong, Wollongong, NSW 2522, Australia  
e-mail: [indra@uow.edu.au](mailto:indra@uow.edu.au)

N. T. Ngo  
e-mail: [trung@uow.edu.au](mailto:trung@uow.edu.au)

Q. Sun  
e-mail: [qideng@uow.edu.au](mailto:qideng@uow.edu.au)

C. Rujikiatkamjorn  
e-mail: [cholacha@uow.edu.au](mailto:cholacha@uow.edu.au)

F. B. Ferreira  
e-mail: [fernanda@uow.edu.au](mailto:fernanda@uow.edu.au)

**Keywords** Ballast · Rail transportation · Synthetic inclusions · Finite element modelling

## 1 Introduction

Rail network forms an important part of the transport system in Australia and many other countries in the world. Railways play a vital role in its economy through transporting freight and bulk commodities between major cities and ports, apart from carrying passengers in commuter trains using the same rail networks, particularly in urban areas. The need to maintain competitive advantages over other transportation modes has increased stresses on the railway industry to enhance its efficiency and decrease maintenance and infrastructure costs (Indraratna et al. 2011a). In the case of ballasted tracks, the cost of maintenance can be decreased if a better understanding of the engineering concepts and mechanisms is obtained in relation to physical and mechanical characteristics of the rail substructure and of the ballast layer in particular.

The ballasted rail track network offers the most demanded and widely used mode of freight transportation in Australia. In order to support track superstructure, the use of a ballast layer is prioritised for several reasons, including construction economics (availability and abundance of materials), ensuring rapid drainage, sufficient bearing capacity, and resiliency to withstand repeated wheel loads (Indraratna et al. 2011a). Upon train loading, ballast grains become degraded by cyclic train loading. The adverse consequences can be the fouling of ballast, causing reduced friction and shear strength (Indraratna et al. 2012, Selig and Waters 1994, Rujikiatkamjorn et al. 2012). The number of studies carried out to assess the adverse effects that fouling has on the shear behaviour of ballast is very limited (Ngo et al. 2014, 2016a, 2017; Budiono et al. 2004, Tutumluer and Dombrow 2008, Indraratna et al. 2013; Rujikiatkamjorn et al. 2013). Upon fouling, the accumulation of fine particles (e.g. coal, subgrade silt, and clay) influences ballast behaviour to make tracks become unstable and misaligned (e.g. differential settlement and localised undrained failure). It is noteworthy that the Australian rail industry spends over hundred millions of dollars in track maintenance and ballast replacement every year.

Since ballasted tracks have minimum transverse lateral support (confinement), the confining pressure must be increased to control lateral deformation (Lackenby et al. 2007, Indraratna et al. 2012, Sun et al. 2016). The mechanical behaviour of ballast is governed by several properties of this granular material such as the particle size distribution (PSD), void ratio, and the corresponding relative density (Indraratna et al. 2011a). It is noted that while the properties of each ballast particle such as size, shape, and angularity affect its degradation response under traffic loading, the deformation is also influenced by the magnitude of axle loads, number of loading cycles, and frequency (Sun and Indraratna 2014; Sun et al. 2016; Selig and Waters 1994, Indraratna et al. 2014b). The magnitudes of the impact forces are dependent on the imperfections on the wheels (long-term wear) and rails (corrugations), as well as on the dynamic responses of the track (Powrie et al. 2007; LePen 2008).

The use of polymeric geosynthetics (geogrids, geotextiles, and geocomposites), shock mats (under ballast mats and under sleeper pads), and recycled rubber tyres can improve the stability and longevity of track, while reducing the annual maintenance costs (Indraratna et al. 2017a). Geogrids have been widely used to reinforce ballasted tracks and also increase the duration of track serviceability (e.g. Bathurst and Raymond 1987; McDowell et al. 2006; Brown et al. 2006; Ngo et al. 2017; Tutumluer et al. 2012). It has been reported that, once they have been placed, the mechanical interlock by geogrids with the surrounding ballast assembly can decrease the lateral displacement and particle degradation (Bathurst and Raymond 1987; Indraratna et al. 2017). In order to obtain greater insight into the performance of geosynthetic inclusions, extensive field trials have been implemented on two specific rail lines in the towns of Singleton, Bulli, located in NSW, Australia, with the support from Australian Rail Track Corporation (ARTC) and Sydney Trains (previously RailCorp) (Indraratna et al. 2010, 2017c). The beneficial effects of geosynthetics and rubber mats were also examined using large-scale laboratory tests subjected to both cyclic and impact loadings. Details of instrumentations, the process of field monitoring, and results measured from these field studies and laboratory tests are presented in the following sections.

With these obvious profits, available research on the geogrid–ballast interface response is limited, albeit some laboratory studies and computational simulations, especially when ballast gets degraded (Indraratna et al. 2011b). Past research has also attempted to use cellular reinforcement to provide additional lateral confinement to the substructure or capping layer with geocell-infilled aggregates (Biabani et al. 2016a). Under the induced loads, additional confinement by the geocell helps to prevent the enclosed aggregates from spreading laterally (Ngo et al. 2016). Also, by increasing the infill rigidity, the geocell could enhance the load-bearing capacity of the track, which in turn enhances its performance in view of load–deformation response (Biabani et al. 2016b; Ngo et al. 2016b). In this paper, the role of geosynthetics and rubber energy-absorbing layers in rail track stabilisation is described based on a series of large-scale laboratory tests involving fresh and fouled ballast, finite element modelling (Indraratna et al. 2011b, 2017a, 2018; Tennakoon et al. 2012; Sun et al. 2016), and data obtained from comprehensive field trials conducted on a instrumented ballasted embankment at Singleton (Nimbalkar and Indraratna 2016).

## 2 Laboratory Tests on Ballast

### 2.1 Ballast Fouling

During train operations, fine particles may fill the voids of ballast aggregates. This can be due to: (i) breakage of ballast sharp edges, (ii) fines infiltrating from the track surfaces, and (iii) fluidisation of soft subgrades (i.e. mud pumping) under extremely high hydraulic gradients caused by cyclic loads (Tennakoon et al. 2012).

As the fouling material occupies the free voids of ballast, it slowly impedes the track drainage capacity. Most ballast fouling (nearly 75%) stems from the breakage and abrasion of the rock grains, 13% due to infiltration from the sub-ballast, 7% migration from the top surfaces, followed by 3% intrusion of subgrade, and 1% comes from sleeper wear (Selig and Waters 1994). In Australia, coal fouling and degradation of ballast are the main sources of fouling materials and they account for about 70–95 and 5–30% (Feldman and Nissen 2002). In coastal track lines, fine silts and clays can be fluidised and pumped up into the ballast aggregates. However, this problem can be eliminated if a properly graded filtration layer or an appropriate geosynthetic filter is placed underneath the ballast layer (Trani and Indraratna 2010; Indraratna et al. 2011a).

## 2.2 Assessment of Ballast Fouling

There are a number of fouling indices available for evaluating the ballast fouling. Selig and Waters (1994) introduced a fouling index (FI) that is the total by mass of fouled ballast passing a 4.75 mm (i.e. No. 4) sieve and 0.075 mm (i.e. No. 200) sieve. Later, Feldman and Nissen (2002) suggested a percentage void contamination (PVC) to overcome some of the limitations associated with FI; PVC is given by the ratio of volume of fines to the void volume of fresh ballast. Since the mass-based index could give an inaccurate estimation of fouling when the contaminating materials (e.g. coal fines) have a relatively small specific gravities, this fouling index has become questionable in certain coal networks. Tennakoon et al. (2012) modified this fouling index by introducing a new fouling index called the Void Contaminant Index (VCI):

$$VCI = \frac{(1 + e_f)}{e_b} \times \frac{G_{sb}}{G_{sf}} \times \frac{M_f}{M_b} \times 100 \quad (1)$$

in which  $e_f$  is void ratio of fouled materials;  $G_{sf}$  is specific gravity of the fouling materials;  $e_b$  is void ratio of ballast;  $G_{sb}$  is specific gravity of ballast;  $M_b$  is weight of ballast; and  $M_f$  is weight of fouling agent. It is noted that there can be a considerable change in the void ratio, but the  $VCI$  can include all of these variations to an acceptable level.

## 2.3 Influence of Ballast Fouling on Track Drainage

Constant head permeability tests were conducted by Tennakoon et al. (2012) at the University of Wollongong (Fig. 1). They measured the hydraulic conductivity for ballast at different amounts of fouling to analyse the relationship between the VCI and the permeability. This permeability equipment is 500 mm diameter and 1000 mm height. A geotextile membrane (i.e. filter) was put above a bottom coarse granular

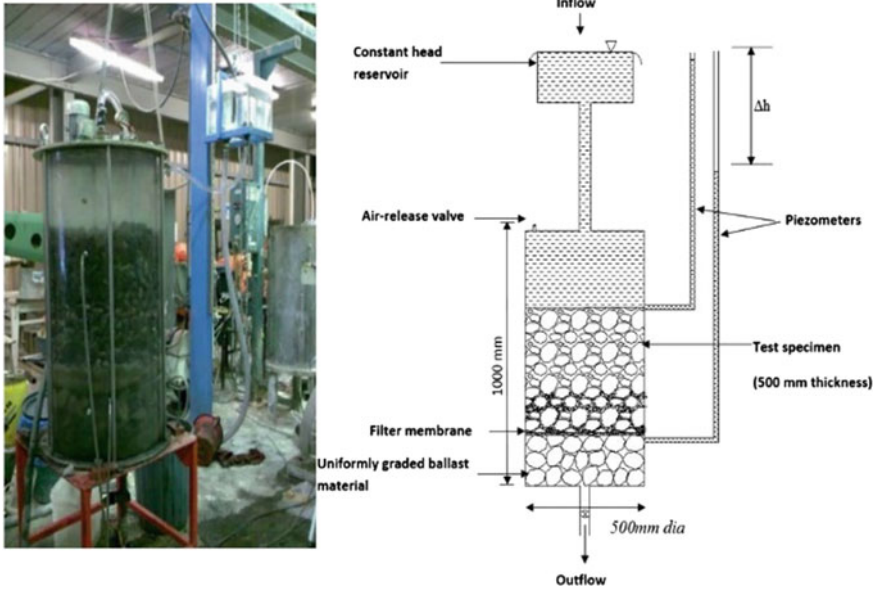


Fig. 1 Permeability test facility used in laboratory

layer while still maintaining a free drainage boundary to prevent fouling material flowing out. The ballast thickness in most rail tracks is commonly between 300 and 500 mm, so a 500-mm-thick ballast layer was used to determine the permeability of fouled ballast. The fouled ballast was placed into the apparatus and compacted in several layers (i.e. equal thickness) to represent a desired density of  $15.5 \text{ kN/m}^3$ . Fouling materials having different gradation curves such as coal fines, commercial kaolin, and clay-fine sand were used to simulate fouled ballast. To mimic a real ballast fouling scenario, the ballast aggregates were compacted and the fouling agents were let to infiltrate downwards by water. For the case of uniformly distributed fouling, predetermined amounts of kaolin corresponding to different degrees of fouling were mixed with ballast and compacted to obtain similar initial density of ballast.

Figure 2 shows that the hydraulic conductivity decreases with increased *VCI*. The laboratory test data reveal that around 5% increased *VCI*s results in a reduction of hydraulic conductivity of at least 200 times and up to 1500 times when ballast is fouled by coal fines and fine silty sands, respectively. It is also observed that the reduced permeability did not influence the required drainage capacity for safe track operations. Once the *VCI* is higher than 75%, a further decrease in hydraulic conductivity is less pronounced as it gets closer to the hydraulic conductivity of the fouling agent.

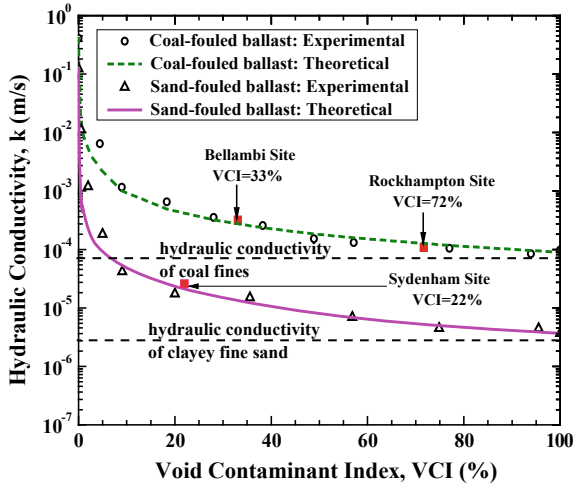


Fig. 2 Evolution of hydraulic conductivity ( $k$ ) at different VCIs. *Data source* Tennakoon et al. (2012)

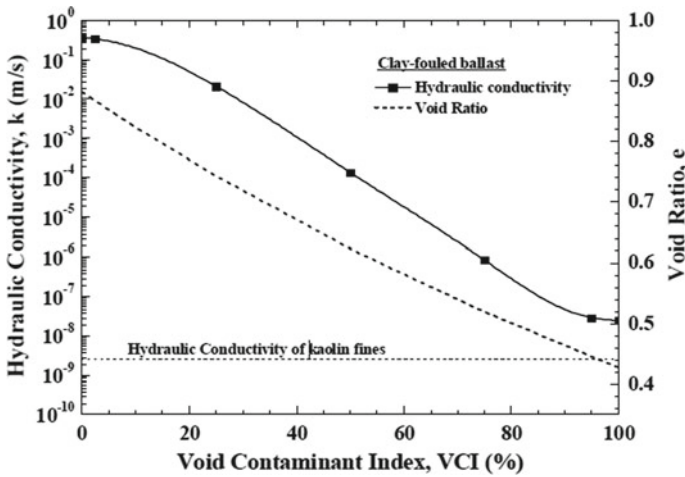


Fig. 3 Changes of hydraulic conductivity with varying VCIs for uniform clay-fouled ballast. *Data source* Tennakoon et al. (2012)

Figure 3 shows the evolution of hydraulic conductivity with increasing  $VCI$  values for clay-fouled ballast. At a small amount of  $VCI$ , hydraulic conductivities of fouled ballast are almost unaffected, but when the  $VCI$  is higher than 90%, the permeability of fouled ballast is significantly reduced and approaches that of pure kaolin.

## 2.4 Large-Scale Direct Shear Tests

A large-scale direct shear box utilised in this study has a plan area of  $300 \text{ mm} \times 300 \text{ mm}^2$  and a height of 200 mm (Fig. 4). The ballast obtained from a quarry near Wollongong was cleaned and mixed in required proportions following the Australian Standards AS 2758.7 (1996). Coal fouling was selected as fouling agents, while the Void Contaminant Index was used to measure the fouling level. Direct shear tests were carried out for both fouled ballast and fresh ballast stabilised by  $40 \text{ mm} \times 40 \text{ mm}$  aperture geogrid to a shear deformation of  $\Delta h = 37 \text{ mm}$ ; and the detailed results were discussed elsewhere by Indraratna et al. (2011b). These test results show that the shear strength of ballast increases with increased normal stresses, while it decreases with increased amount of fouling. Strain softening has also been recorded for all the tests. For a higher normal stress  $\sigma_n$ , a greater peak shear stress and reduced dilation were observed.

Figure 5 shows that fouling agents decrease the shear strength of unreinforced and reinforced ballast specimens by coating the aggregates surfaces, thus reducing the interparticle friction while inhibiting the shearing constraint of the composite assemblies. Tutumluer et al. (2008) found that the ballast aggregates they tested in the laboratory had alike stress–strain responses. The evolutions of normalised maximum shear stress ( $\tau_p/\sigma_n$ )(a friction angle,  $\phi$  (apparent angle) versus *VCI* for fouled/fresh ballast specimens considering the role of geogrid reinforcement are shown in Fig. 5. Note that the coal fines considerably reduce the maximum shear stress and decrease the friction angle of the fouled ballast. When the *VCI* is smaller than 70%, the reduction of ( $\tau_p/\sigma_n$ ) due to the fines is significant, but it has marginal effect when the *VCI* is greater. The measured apparent friction angles of the unreinforced ballast varied from  $46^\circ$  to  $65^\circ$  depending on the applied normal stress. It is believed that the friction of ballast decreases with increased confining pressure, and this trend is similar to that of unreinforced/reinforced ballast.

## 2.5 Geogrid–Ballast Interface Behaviour

The influence of the grid geometry, opening size of geogrid, and the confining pressure on the interface behaviour of a geogrid-reinforced ballast assembly was evaluated by Indraratna et al. (2012). In this study, seven geogrids (*G1–G7*, Table 1), having rectangular, square, and triangular opening aperture (i.e. 36–70 mm), were tested under various normal stresses (15–75 kPa). All the specimens were subjected to a lateral deformation of 36 mm, corresponding to a horizontal shearing strain of 12%.

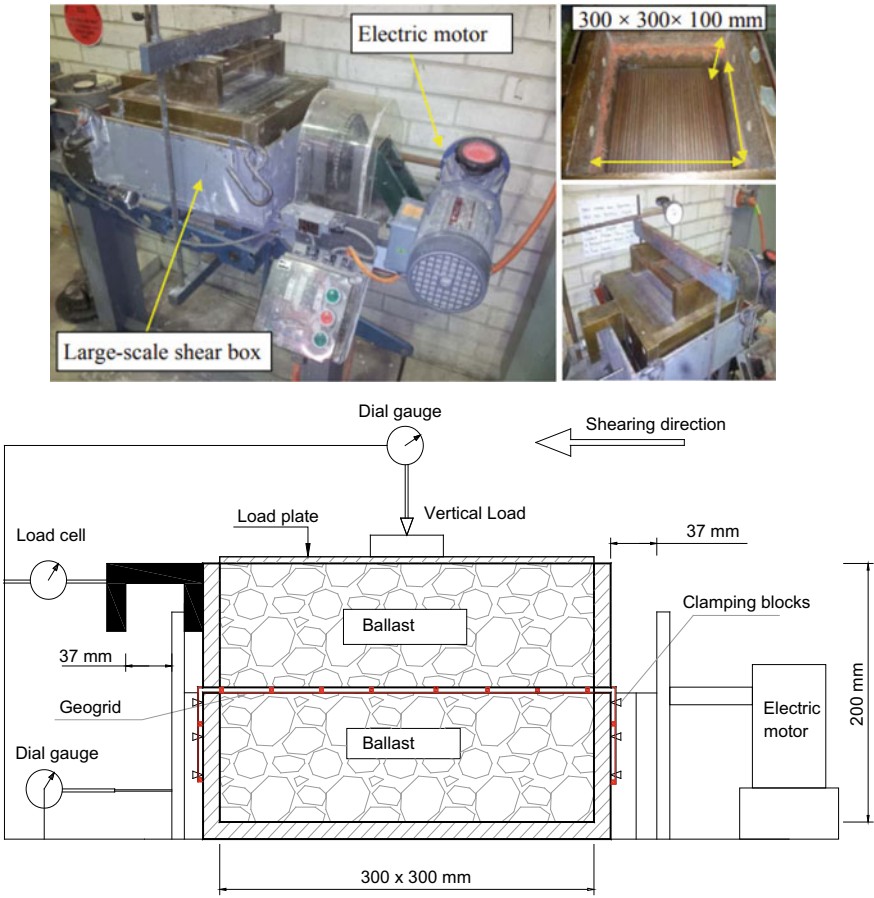


**Fig. 4** Large-scale direct shear box

The actual effectiveness of the ballast–geogrid interaction can be quantified via an interface efficiency factor ( $\alpha$ ). This factor can be computed as:

$$\sigma = \frac{\tan \delta}{\tan \phi} \tag{2}$$

where  $\phi$  is ballast friction angle and  $\delta$  is ballast–geogrid interface friction angle.

The effect of the geogrid opening size ( $A$ ) on the shear strength of geogrid-reinforced ballast specimens is presented in Fig. 6, where  $\alpha$  values are plotted as a function of the  $A/D_{50}$  ratio. It is observed that  $\alpha$  raises with increased  $A/D_{50}$  until it reaches a highest value of 1.16 when  $A/D_{50}$  is 1.21. The  $\alpha$  value decreases as  $A/D_{50}$  comes close to 2.5. When  $\alpha < 1$  shows a reduced interlocking among aggregates, whereas  $\alpha > 1$  implies a reasonable interlocking, which contributes to an increase



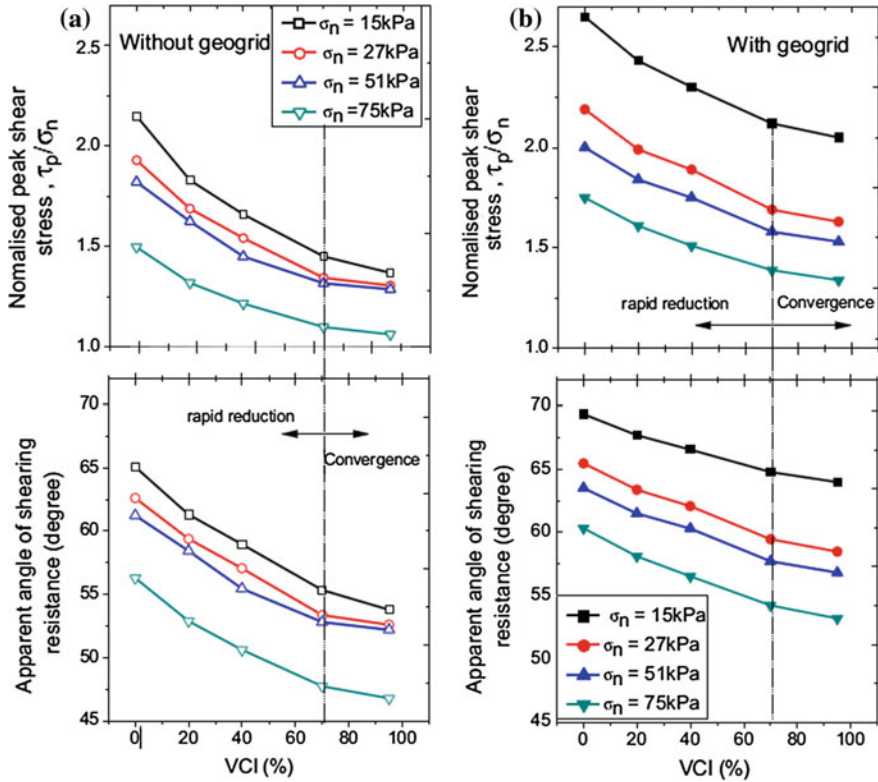


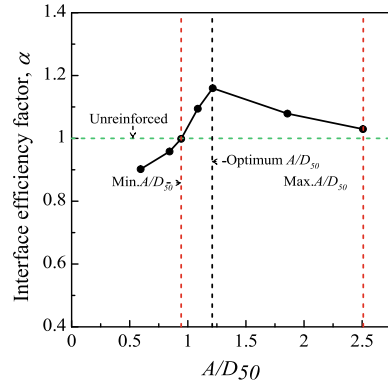
**Fig. 5** Influence of VCI on shear strength and frictions of ballast specimens: **a** no geogrid; **b** with geogrid. *Data source* Indraratna et al. (2011b)

**Table 1** Physical data of the various geogrids tested

Geogrid type	Aperture shape	Aperture size (mm)	Tensile strength (kN/m)
Grid 1	Square	38 × 38	30
Grid 2	Triangle	36	19
Grid 3	Square	65 × 65	30
Grid 4	Rectangle	44 × 42	30
Grid 5	Rectangle	36 × 24	30
Grid 6	Square	33 × 33	40
Grid 7	Rectangle	70 × 110	20

*Data source* Indraratna et al. (2012)

**Fig. 6** Interface efficiency factor ( $\alpha$ ) versus  $A/D_{50}$ .  
Data source Indraratna et al. (2012)



of peak shear stresses. This study implies that the geogrid opening aperture sizes to optimise the shear strength are  $0.95D_{50}$  and  $2.50D_{50}$ , respectively, and the optimum aperture size is approximately 1.2–1.3 times the value of  $D_{50}$ .

## 2.6 Large-Scale Triaxial Tests for Ballast Subject to Various Frequencies

The effect of varied frequencies (i.e. train speeds) on the ballast degradation and deformation when subjected to dynamic train loads has been examined using a novel large-scale cylindrical triaxial test facility (Fig. 7). The ballast specimens have been consolidated under lateral confinements ( $\sigma_3'$ ) of 10, 30, and 60 kPa. Frequencies ( $f$ ) ranging from 5 to 60 Hz were tested to resemble train speeds of 40–400 km/h. Maximum cyclic deviatoric stresses ( $q_{\max, \text{cyc}}$ ) of 230–370 kPa were applied to simulate axle train loading of 25–40 tonnes.

Figure 8 shows the evolution of axial strains ( $\varepsilon_a$ ) with increased load cycles ( $N$ ) under varying loading amplitudes ( $q_{\max, \text{cyc}}$ ) and varying frequencies ( $f$ ). It is seen that for a given value of  $f$ , the value of  $\varepsilon_a$  increases with  $N$ . Also, for varying values of  $f$ ,  $\varepsilon_a$  increases with the increase of  $f$  at any given  $N$ . Laboratory test data indicate that four stages of deformation exist under cyclic loads: (i) elastic shakedown; (ii) plastic shakedown with some accumulation of permanent strains; (iii) ratcheting zone where significant accumulation of plastic strains is observed; and (iv) plastic collapse, as described by Sun et al. 2016. Correspondingly, three stages deformation were identified with the variation of frequency of loading, including Range I, at  $f \leq 20$  Hz—plastic shakedown; Range II, for  $30 \text{ Hz} \leq f \leq 50 \text{ Hz}$ —plastic shakedown and ratcheting; and Range III, for  $f \geq 60 \text{ Hz}$ —plastic collapse, as illustrated in Fig. 5a, b. The frequency  $f$  applied in these triaxial tests could be converted to equivalent train speed  $V$  based on standard gauge track geometry (Indraratna et al. 2011a). Cyclic testing data reported by Lackenby et al. (2007) also emphasized the

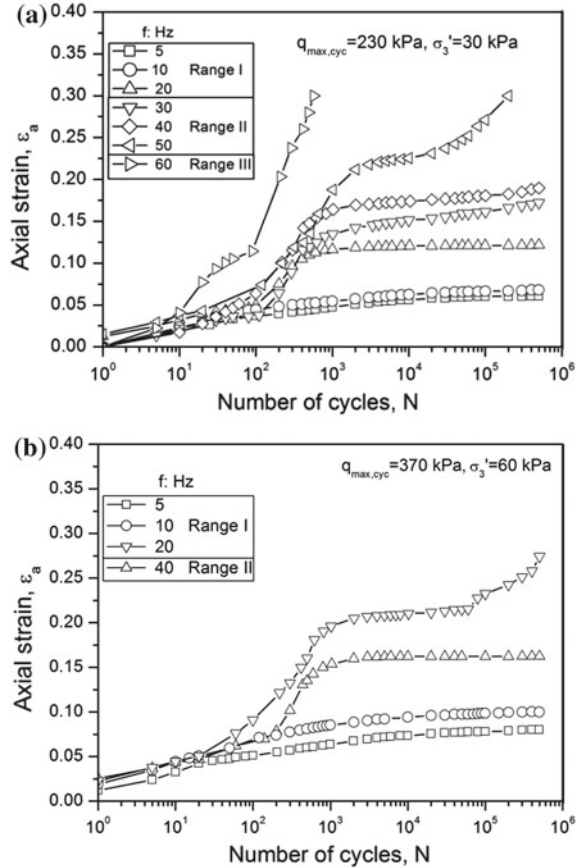


**Fig. 7** Large-scale triaxial test facility at UOW

coexist of identical stages of ballast deformation behaviour based on the stress ratio ( $q_{\max, \text{cyc}}/p'$ ).

Different ballast degradation characteristics were identified according to varying deformation stages during loading tests (Fig. 9). In Range I,  $f \leq 30$  Hz, corner breakage and attrition of asperities were the major forms of particle degradation. In Range II,  $30 \text{ Hz} < f < 60 \text{ Hz}$ , particle splitting due to fatigue and particle attrition associated with increased vibration were predominant. In Range III,  $f \geq 60 \text{ Hz}$ , particle splitting occurred due to decreased coordination number.

**Fig. 8** Evolutions of axial strains versus load cycles:  
**a**  $q_{max,cyc} = 230$  kPa and  
**b**  $q_{max,cyc} = 370$  kPa  
 (modified after Sun et al. 2016)



### 3 Performance of Rubber Tyre-Confined Capping Layer for Railroad Conditions

#### 3.1 Description of Testing Materials and Test Procedure

Cyclic triaxial tests were done using a prototype process simulation prismatic triaxial apparatus (PSPTA—Fig. 10). The bottom layer was compacted by a 50-mm-thick rockfill, followed by a 200-mm-thick sub-ballast layer was filled. Two types of ballast including fresh crushed basalt and recycled aggregates were tested with and without the inclusion of recycled tyres. A woven geomembrane was put under the rubber tyres as a separator. Strain gauges were installed on interior walls of the scrap tyres to record mobilised strains in axial and circumferential directions. The upper segment consisted of fresh ballast. A concrete tie (sleeper) and rail assembly was installed above the ballast layer, and then, the gaps between sleeper and walls were



**Fig. 9** Typical images of particle breakage (modified after Sun et al. 2016)

placed by additional aggregates. Whereas the 200-mm-thick sub-ballast layer was compacted in two layers of 100 mm thickness, the 300-mm-thick ballast stratum was compressed in every 75-mm-thick layers to attain their representative unit weight in the field. These materials were compacted using a vibratory hammer. The set-up for this specimen is shown in Fig. 11.

The above tests utilised  $\sigma'_{1\text{cyc}} = 370$  kPa to simulate the vertical stress generated from a static heavy haul train having a maximum axle load of 40 tonnes. The load frequency is generally described by  $f = V/L$ , in which  $V$  is train speed and  $L$  is length between the closest sets of axles in a given freight train. Therefore, for the smallest distance between axles of 2.02 m between an adjacent set of bogies, the frequency is around 0.138 V; hence, a value of  $f = 15$  Hz represents a maximum train speed of approximately 110 km/h.

To mimic actual track conditions, a relatively small lateral pressure  $\sigma'_3 (= \text{kPa})$  was applied to the assembly by hydraulic jacks. Every test was carried out to  $N = 500,000$  cycles. After completing each test, the ballast was then sieved to calculate the amount of breakage according to the BBI—ballast breakage index proposed by Indraratna et al. 2005.

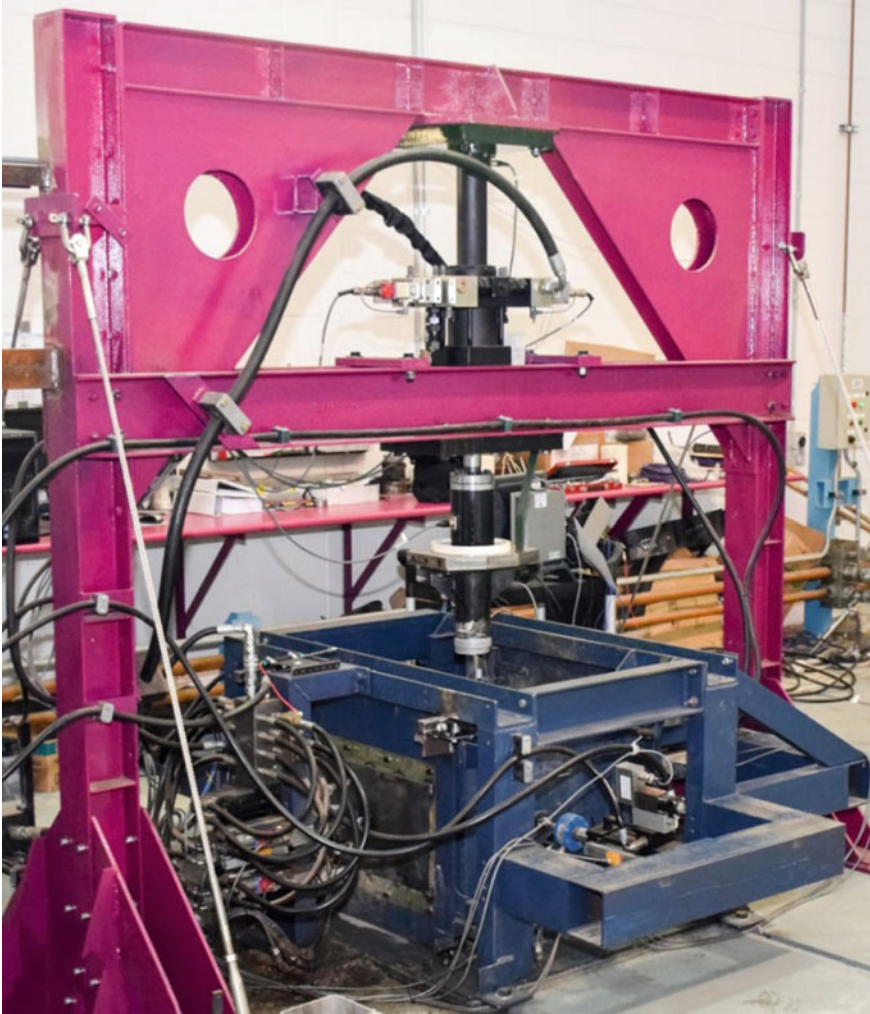
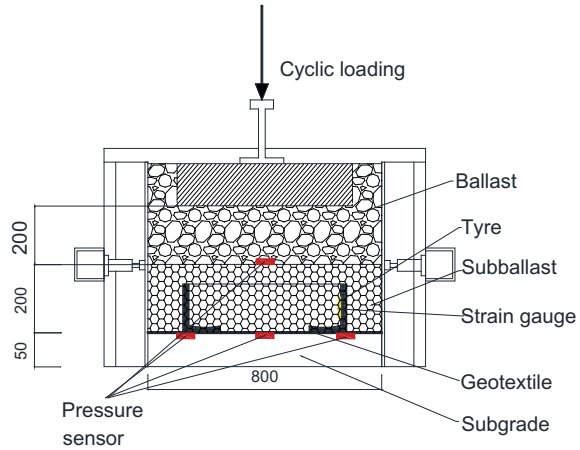


**Fig. 10** Process simulation prismoidal triaxial apparatus (photograph taken at SMART Rail lab-UOW)

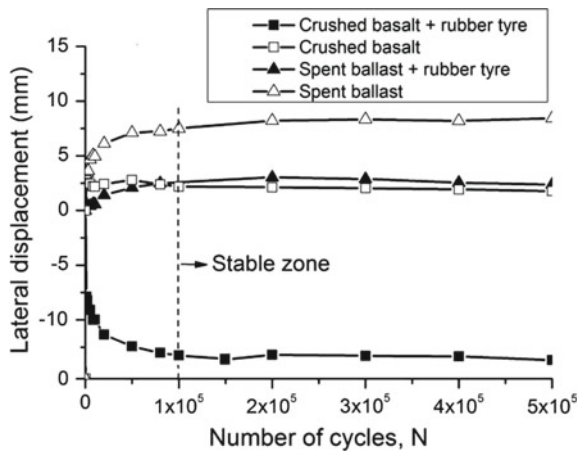
### ***3.2 Results and Discussion***

Figure 12 shows the evolution of the lateral displacements of the specimens with the number of cycles. As expected, the lateral movement of the specimens tested without tyre confinement increased rapidly for a small number of loading cycles and then stabilised at  $N = 100,000$  cycles. Furthermore, the specimens confined with the rubber tyre cell infilled with spent ballast exhibited a substantial reduction in the lateral spreading (approximately 60%), whereas the tyre cell specimens infilled

**Fig. 11** Schematic illustration of process simulation prismoidal triaxial apparatus (dimensions in mm)



**Fig. 12** Variation of lateral displacement of specimens versus load cycle. Data source Indraratna et al. (2018) with permission from ASCE



with a finer (crushed) basalt mainly compressed laterally. This is not surprising as under cyclic loads granular materials are compressed vertically and are expected to spread laterally; however, the rubber tyre cell can provide additional confinement to the infilled materials, thus minimising their lateral displacement. In addition, visual inspection during the tests showed that the ballast particles around the sleeper (Fig. 11) moved upwards under vibration loading, and the vertical boundaries of the specimen were pushed inwards by the constant lateral pressure  $\sigma'_3$  (=kPa) applied by the hydraulic jacks.

During service, railway ballast undergoes significant changes in stress because of repeated cyclic and impact loading and also experiences considerable particle breakage (Indraratna et al. 2011a). The fresh ballast directly under the tie (sleeper) was painted white (Fig. 13a) to conveniently determine the BBI after each test. Various ballast breakage modes such as the attritions and corner breaks

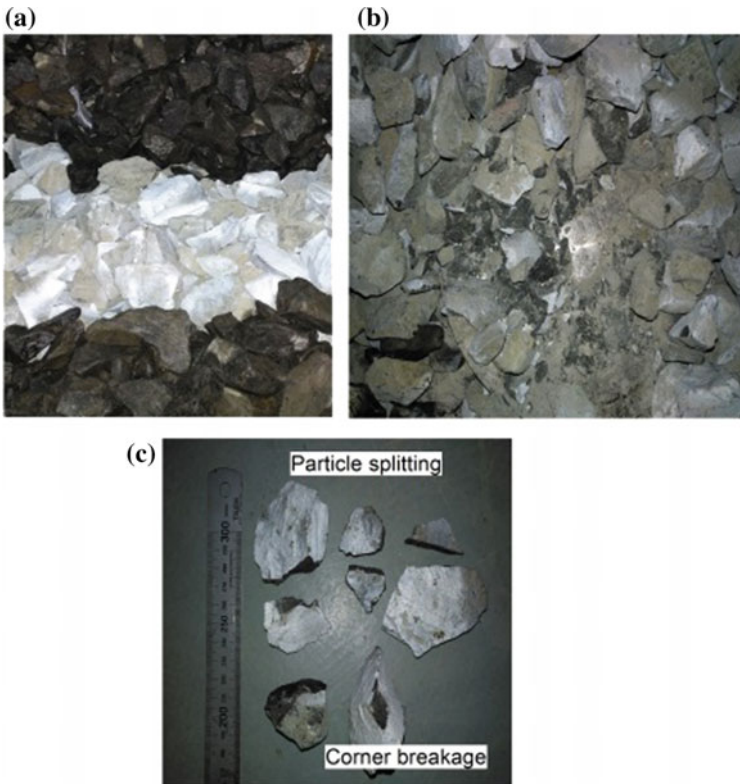


**Fig. 13** **a** Fresh ballast before test; **b** degraded ballast after test, and **c** examples of particle degradation modes (after Indraratna et al. 2018)

(Fig. 13b, c) and particle splitting (Fig. 13c) occurred after cyclic loading. Figure 14 compares the PSD curves of the samples before and after each test, whereby the values of BBI are smaller for the specimens having a rubber tyre cell. This indicates that the use of a rubber tyre cell to confine the capping layer can effectively reduce ballast degradation, as such a system has a higher capacity to attenuate the energy which in turn could improve the overall track longevity.

## 4 FEM Modelling for Tracks with Tyres

### 4.1 Description of the FEM Model

A plane strain (transverse) cross section of a rail track was simulated by FEM to evaluate the ballast lateral deformation and the subgrade (natural soil foundation)



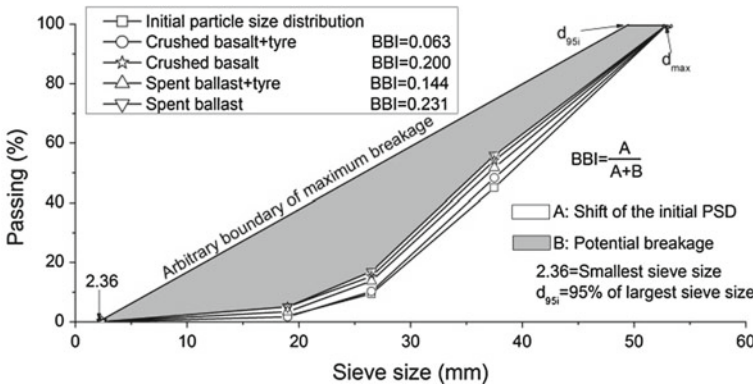


**Fig. 14** PSD curves before and after cyclic loading. *Data source* Indraratna et al. (2018)-with permission from ASCE

stress with and without rubber tyres reinforcing the capping layer. The FEM model with the inclusion of rubber tyres is shown in Fig. 15.

The ballast, sub-ballast (capping), and subgrade were considered as elastoplastic following to Mohr Coulomb failure criterions. The scrap tyres were simulated as a cylinder. The rails and sleepers were taken as linear elastic materials, whose considerably higher stiffness in comparison to the rubber tyres, ballast, and subgrade

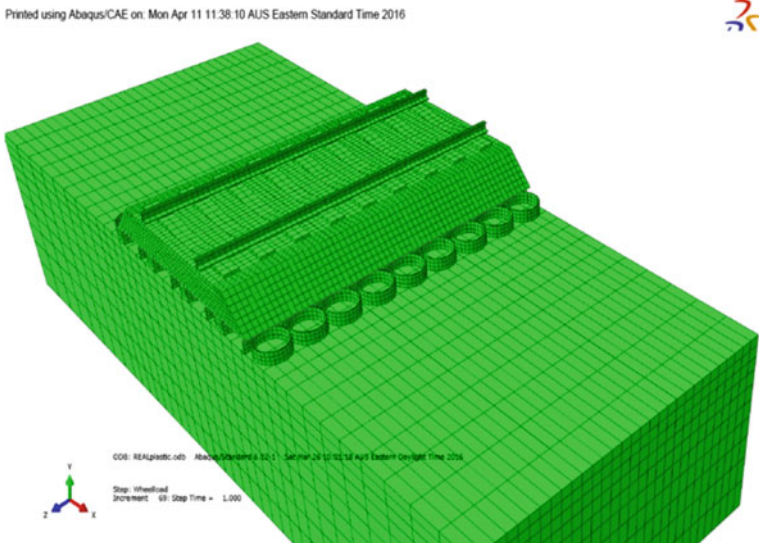


**Fig. 15** FE mesh of a ballasted rail track with inclusion of rubber tyres

mimicked a composite layered structure of varied stiffness with depth. The values of model parameters used in the FEM simulation are shown in Table 2.

It may be argued that to simulate a track substructure, a true 3D-FEM would be more appropriate, but the track is very long, and therefore, it can be assumed as plane strain conditions that could be done by applying correct boundary constraints. In the current analysis, the width of the model was simulated as 1.9 m, and given the symmetry of its geometry, only half of typical tracks were considered. Ballast and subgrade layers were simulated by meshes composed of C3D8R, as described by Abaqus manual. In order to resemble the conditions prevailing in the field, the plane strain criterion was imposed, where the longitudinal deformations were considered insignificant when compared to the transverse strains. The outside vertical planes of the model were fixed from any horizontal movements (i.e. transverse directions), and the same conditions were applied to the  $xy$ -planes to restrict horizontal movement in  $z$ -directions. The bottom of the track was fixed (non-displacement boundary), as typically needed for a FEM model.

## 4.2 Model Predictions

Railway design often ensures that the traffic load acting on the subgrade is kept within limits that can avoid excessive shear failure and/or significant plastic deformations of the subgrade (Li and Selig 1998), as well as reducing the degradation and dilation of the track substructure materials including ballast and subballast (Indraratna et al. 2011a). To keep track alignment, ballast horizontal strains should be kept within specific ranges. It is therefore important to understand how the ballast lateral spreading and subgrade stress can be affected by the inclusion of rubber tyres in the capping layer, as opposed to the unreinforced case.

Figure 16 shows that the lateral strains along the slope of the track embankment could be significantly reduced by the use of tyre reinforcement. The lateral displacement contours for tyre-reinforced and unreinforced layers of subballast are presented in Fig. 17. It can be seen that for the reinforced case, the largest lateral displacement occurs underneath the sleeper edge. This analysis also indicates that the highest horizontal movements for the unreinforced subballast layer (0.1 m) was significantly larger than that of the reinforced sub-ballast (0.01 m) subjected to the same loading conditions.

The influence of the reinforcement provided by end-of-life tyre on the stresses acting at the interface between the subballast and the subgrade is illustrated in Fig. 18. As expected, the largest deviatoric stresses develop close to sleeper edges and then they decrease to the centre of the sleepers. This is in agreement with data measured in the field where the highest settlements typically take place near the sleeper edges (Li and Selig 1998). In the presence of waste tyres, a train with a given axle load operating at a certain speed induces a maximum deviator stress on the subgrade that is almost 12% less than that in the absence of the reinforcement. Intuitively, the confining effect provided by the recycled tyres causes the tyre-infilled gravel composites acting as

**Table 2** Values of model parameters used in the FEM analysis (after Indraratna et al. 2017a)

Track parameters	Values
<i>Parameters for rails</i>	
Density	2000 (kg/m <sup>3</sup> )
Young's modulus $E$	500,000 (MPa)
Poisson's ratio, $\nu$	0.30
<i>Parameters for sleepers</i>	
Density	2000 (kg/m <sup>3</sup> )
Young's modulus $E$	30,000 (MPa)
Poisson's ratio, $\nu$	0.25
<i>Parameters for ballast aggregates</i>	
Density	1530 (kg/m <sup>3</sup> )
Young's modulus $E$	200 (MPa)
Poisson's ratio, $\nu$	0.30
Friction angle, $\phi$	45°
Dilation angle, $\psi$	15°
Cohesion	1 (kPa)
Thickness of ballast	350 mm
<i>Parameters for sub-ballast</i>	
Density	2100 (kg/m <sup>3</sup> )
Young's modulus $E$	2000 (kPa)
Poisson's ratio, $\nu$	0.3
Friction angle, $\phi$	39°
Dilation angle, $\psi$	15°
Cohesion, $c$	1.0 (kPa)
<i>Parameters for subgrade</i>	
Density	1700 (kg/m <sup>3</sup> )
Young's modulus, $E$	2000 (kPa)
Poisson's ratio, $\nu$	0.30
Friction angle, $\phi$	40°
Dilation angle, $\psi$	15°
Cohesion, $c$	5.0 (kPa)
<i>Parameters for scrap tyres</i>	
Density	1500 (kg/m <sup>3</sup> )
Young's modulus, $E$	750 (MPa)
Poisson's ratio, $\nu$	0.35

(continued)

**Table 2** (continued)

Track parameters	Values
<i>Parameters for wheel loads</i>	
Static loads	122.5(kN)
Train velocity	100 (km/hour)
Dynamic amplification factors (DAFs)	1.540
Dynamic wheel loads	188.2 (kN)
<i>Parameters for interface</i>	
Normal properties	Hard contact
Tangential coefficients	0.450

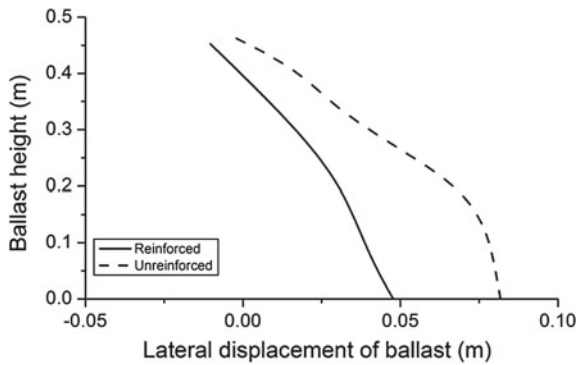


**Fig. 16** Horizontal movements of ballast. *Data source* Indraratna et al. (2017b)

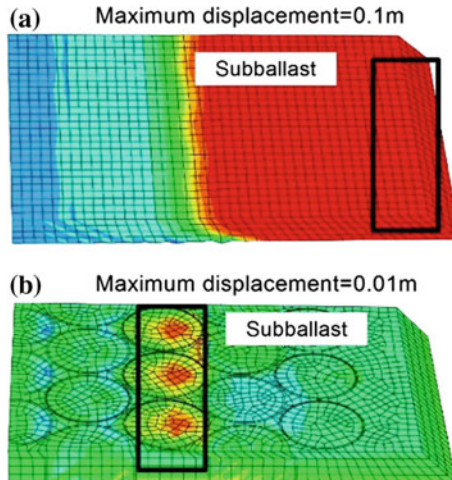


**Fig. 17** Maximum lateral displacement in the subballast layer: **a** without rubber tyres and **b** with rubber tyres (after Indraratna et al. 2017b)

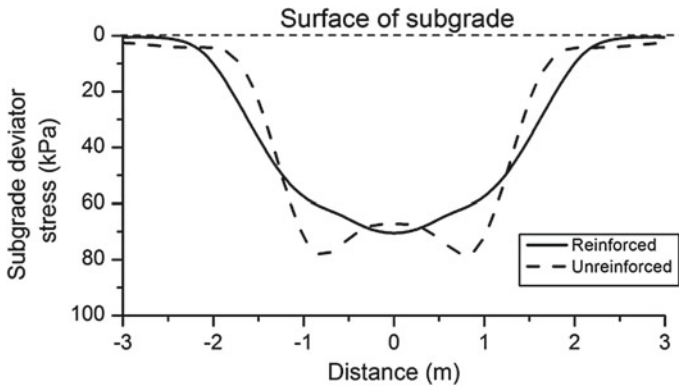


**Fig. 18** Stress distributions on subgrade (after Indraratna et al. 2017b)

a stiffer layer that enables more uniform stress distribution to be transferred to the underlying subgrade layer. Figure 18 also suggests that the induced subgrade stresses can be distributed over a wider area when the tyre reinforcement is included.

## 5 Use of Geogrids and Shock Mats

### 5.1 Field Study: Singleton Track

To assess the benefits of using geogrids and rubber mats in rail tracks, a field test was implemented in the town of Singleton, located at about 200 km from Sydney (Nimbalkar and Indraratna 2016; Indraratna et al. 2016).

### 5.2 Construction of Singleton Tracks

The track substructure was composed of a 300-mm-thick ballast layer underlain by a sub-ballast having 150–300 mm thickness. A 400–600-mm-thick structural fill was placed below the capping layer. Eight instrumented sections were constructed and monitored for a period of 5 years. The locations of the experimental sections along the track are illustrated in Fig. 19. In order to examine the effect of the subgrade type on the overall performance of geogrid reinforcement, these experimental sections were built on distinct subgrade types, namely (i) Section B—stiff bridge deck with reinforcement; (ii) Sections C and 5—intermediate siltstones; and (iii) Sections A and 1 to 4—soft alluvial with silty-clay deposits.

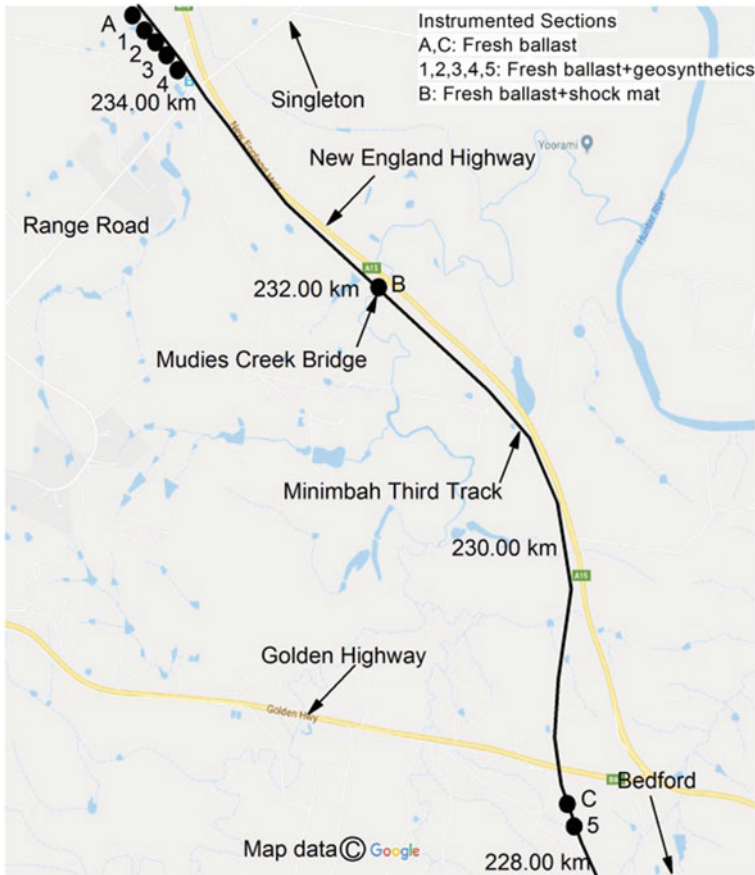


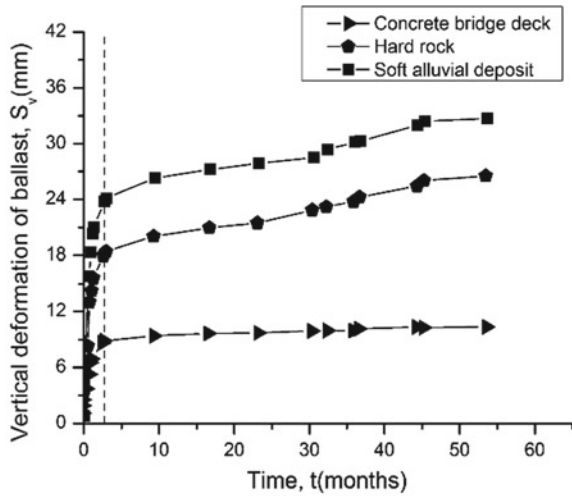
**Fig. 19** Map of the Singleton tracks (after Indraratna et al. 2014a)

Three different geogrids were used for Sections 1, 3, 5. In addition, a layer of under ballast mat (UBM) was placed for Section B—ballast deck bridge. The physical and mechanical properties of the used geogrids and UBM can be found in Nimbalkar and Indraratna (2016).

### 5.3 Deformation of Ballast

The permanent vertical deformations of the ballast layer were estimated by subtracting the settlements at the ballast–sub-ballast from that at the top surface of ballast layer. A comparison of the vertical settlements measured at experimental sections without reinforcement and under different subgrade conditions is given in Fig. 20. It

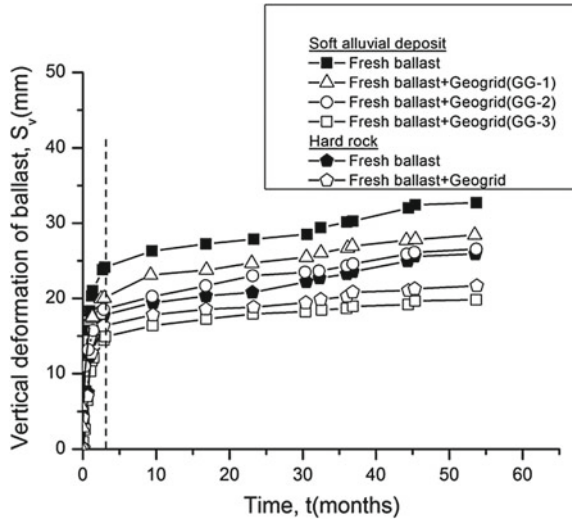
**Fig. 20** Vertical deformations of ballast layer for varying subgrade types. Data source from Nimbalkar and Indraratna (2016)



is observed that the vertical settlement increased rapidly and was more pronounced under softer subgrade conditions; i.e., the lowest ballast deformations were obtained on the concrete bridge, whereas the largest deformations were measured at track sections involving a silty-clay foundation. The low deformation at the bridge (Muddies Creek) may result from the confinement provided to the ballast by the bridge barriers and from the use of rubber mat, which led to reduced lateral movements of ballast. However, at other places, ballast particles could move freely in the lateral directions, which in turn caused larger vertical deformations.

The permanent vertical deformations of geogrid-reinforced ballast were 5–35% smaller than those in the absence of reinforcement, as shown in Fig. 21. This behaviour was also seen by laboratory studies (Ngo et al. 2017b; Indraratna and Salim 2003; Indraratna and Nimbalkar 2013; Göbel et al. 1994; Indraratna et al. 2016) and others (Fernandes et al. 2008) and can be justified by the additional internal confinement resulting from ballast–geogrid interlocking. It was also noticed that the effectiveness of the geogrid reinforcements in reducing ballast deformations was higher under softer subgrade conditions. This finding is consistent with the test data presented by Ashmawy (1995). Moreover, the geogrid (GG-3) usually exhibited the most effectively with respect to the attenuation of ballast strains associated with its aperture ( $D_{50} = 40$  mm) that promoted strong interlock among the ballast grains and geogrids, i.e. increased the interface friction (Indraratna et al. 2014b). Conversely, the aperture size of GG-2 ( $1.8D_{50} = 65$  mm) was too large to enable effective interlock with the ballast commonly adopted in Australian tracks.

**Fig. 21** Vertical deformations of ballast layer for varying reinforcement types *Data source from Nimbalkar and Indraratna (2016)*



### 5.4 Ballast Breakage

To analyse the extent of particle breakage upon repetitive train loading, ballast samples were collected from various places along the tracks during the intermittent periods of closure. A sampling pit ( $1.80 \times 1.30$  m) was obtained by excavating ballast particles from the load-bearing, cribs, and shoulders of the track. The ballast was obtained from three identical locations between the base of sleepers and formation levels and was recovered based on recommendations of AS 1141.3.1 (2012). The ballast profile was subsequently restored by installing fresh ballast which was compacted by tamping heads.

The particle breakage was assessed using the BBI and presented in Fig. 22. The value of BBI for ballast layers stabilised with the geogrid GG-3 was approximately 35% lower than one for non-reinforced sections, indicating geogrids could attenuate the ballast degradation. Even though the train velocities for all sections were nearly the same, the presence of under ballast mat at the concrete bridge deck resulted probably in a reduced amount of breakage ( $BBI < 5\%$ ). As expected, particle breakage was more significant for the hard subgrade when compared to one measured for soft subgrade.

## 6 Conclusions

This paper encapsulates the research works conducted on railroad geomechanics that obtained from advanced large-scale testing and field studies carried out at UOW over the past twenty years. The application of geogrids and recycled rubber mats



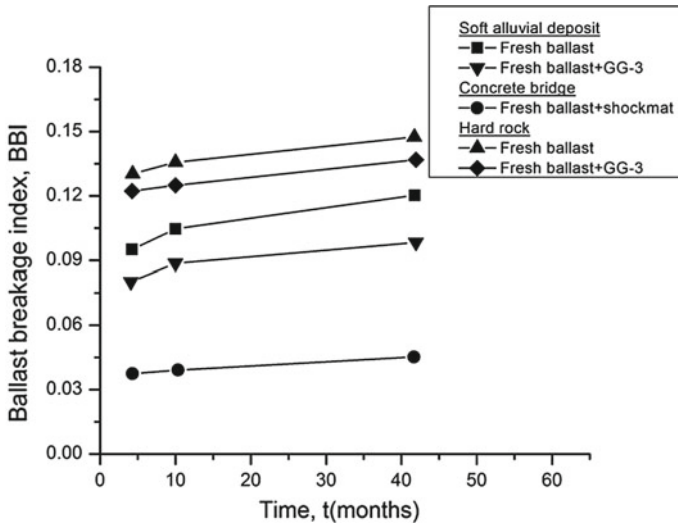


Fig. 22 Variation of BBI with time for different subgrade conditions. Data source from Nimbalkar and Indraratna (2016)

to enhance rail track performance has been analysed together with numerical modelling. Large-scale permeability tests were carried out under varying levels of ballast contamination to establish the relationship between the VCIs and the corresponding hydraulic conductivities. The results showed a decrease in the hydraulic conductivities associated with an increase in the VCI. A serious condition with respect to track maintenance would be reached when VCI was higher than 40% for clay-fouled ballast and 60% for coal fouling.

Large-scale direct shear test for fresh/fouled ballast, both with and without geogrid reinforcement, was implemented to evaluate the shear stress–strain responses and volumetric changes. The test data indicated that the geogrid increased shear strengths and friction angles, while only marginally reducing the vertical deformation of the geogrid-stabilised ballast specimens. When the ballast was fouled, the efficiency of the geogrids reduced in proportion to the amount of fouling. Based on these tests, the optimum opening aperture of grids to provide a maximum interface shear strength was about  $1.20D_{50}$ .

The use of rubber tyre cells for capping (sub-ballast) layer provides considerable lateral confinement to the infilled materials, thus contributing to a reduction in the lateral spreading of particles, hence overall dilation of subballast. In addition, the results of the study showed that a sub-ballast layer stabilised with scrap tyres could effectively eliminate the degradation and vertical movement of the overlying ballast layer.

The improved field performance of a ballasted track in Singleton using geogrids and rubber shock mats was most encouraging. The track performance was examined through a fully instrumented track section employing different types of geogrids

and rubber mats. The field results indicated that the geogrids decreased the ballast settlement by approximately 35%. This would have a considerable reduction of the maintenance costs. The reduction in vertical strains was observed to be higher under softer subgrade conditions. Ballast aggregates experienced considerable breakage due to more intensive train loadings, especially over concrete bridge decks where the placing of rubber shock absorbing mats is highly recommended. The enhanced geogrid-stabilised ballast interactions increased lateral confinements of sub-ballast by tyre cells or geocells, and the placing of rubber mats resulted in more stable tracks with enhanced longevity and stability.

**Acknowledgements** Research projects on ballasted rail tracks as presented in this keynote paper were supported by the Australian Research Council (ARC) and three consecutive Cooperative Research Centres (CRCs) for railways over the past two decades. The authors gratefully acknowledge the efforts of Dr. Syed K. Hussaini, Dr. Nayoma Tennakoon, Dr. Mahdi Biabani, Dr. Joanne Lackenby, and Dr. Sanjay Nimbalkar that have contributed to the contents of this paper. The support and efforts of colleague A/Prof Jayan Vinod and Dr. Ana Heitor over the past years are also appreciated.

The authors greatly appreciate the financial support from the Rail Manufacturing Cooperative Research Centre (funded jointly by participating rail organisations and the Australian Federal Government's Business Cooperative Research Centres Programme) through Project R2.5.1—*Performance of recycled rubber inclusions for improved stability of railways* and Project R2.5.2—*Application of geogrids for minimising track deformation and degradation under high frequency cyclic and heavy haul loading*. The authors wish to thank the Australasian Centre for Rail Innovation (ACRI), Tyre Stewardship Australia (TSA), Global Synthetics Pty Ltd., Naue GmbH & Co. KG, Foundation Specialists Group, Sydney Trains (formerly RailCorp), and Australian Rail Track Corporation for the financial support. The cooperation of David Christie (formerly Senior Geotechnical Consultant, RailCorp), Tim Neville (ARTC), and Michael Martin (Aurizon/QLD Rail) during these industry linkages is gratefully acknowledged. Salient contents from these previous studies are reproduced herein with kind permission from the original sources, including ASCE, CGJ, Geotextiles and Geomembranes, Geotechnical Testing Journal, among others. The authors are also grateful to UOW technical staff, namely Alan Grant, Cameron Neilson, Duncan Best, and Ritchie McLean for their assistance during laboratory and field studies.

## References

- AS 2758.7 (1996) Aggregates and rock for engineering purposes—Part 7: Railway Ballast, Standard Australia, Sydney, NSW, Australia
- AS 1141.3.1 (2012) Methods for sampling and testing aggregates—Method 3.1: sampling-aggregates, Sydney, NSW, Australia
- Ashmawy B (1995) Geosynthetic-reinforced soils under repeated loading: a review and comparative design study. *Geosynthetics Int* 2(4):643–678
- Bathurst RJ, Raymond GP (1987) Geogrid reinforcement of ballasted track. *Transp Res Rec* 1153:8–14
- Biabani MM, Indraratna B, Ngo NT (2016a) Modelling of geocell-reinforced subballast subjected to cyclic loading. *Geotext Geomembr* 44(4):489–503
- Biabani MM, Ngo NT, Indraratna B (2016b) Performance evaluation of railway subballast stabilised with geocell based on pull-out testing. *Geotext Geomembr* 44(4):579–591
- Brown SF, Thom NH, Kwan J (2006) Optimising the geogrid reinforcement of rail track ballast. In: Railfound conference, Birmingham

- Budiono DS, McSweeney T, Dhanasekar M, Gurung N (2004) The effect of coal dust fouling on the cyclic behaviour of railtrack ballast. In: *Cyclic behaviour of soils and liquefaction phenomena*. Taylor & Francis Group, London
- Feldman F, Nissen D (2002) Alternative testing method for the measurement of ballast fouling. In: *Conference on Railway Engineering, Wollongong, RTSA*
- Fernandes G, Palmeira M, Gomes RC (2008) Performance of geosynthetic-reinforced alternative subballast material in a railway track. *Geosynthetics Int* 15(5):311–321
- Göbel W, Kirschner RA (1994) Effectiveness of a reinforced geogrid in a railway subbase under dynamic loads. *Geotext Geomembr* 13(2):91–99
- Indraratna B, Salim W (2003) Deformation and degradation mechanics of recycled ballast stabilised with geosynthetics. *Soils Found* 43(4):35–46
- Indraratna B, Lackenby J, Christie D (2005) Effect of confining pressure on the degradation of ballast under cyclic loading. *Géotechnique* 55(4):325–328
- Indraratna B, Hussaini SKK, Vinod JS (2012) On the shear behaviour of ballast-geosynthetic interfaces. *Geotech Test J* 35(2):1–8
- Indraratna B, Salim W, Rujikiatkamjorn C (2011a) *Advanced rail geotechnology—ballasted track*. CRC Press, Taylor & Francis Group, London, UK
- Indraratna B, Ngo NT, Rujikiatkamjorn C (2011b) Behavior of geogrid-reinforced ballast under various levels of fouling. *Geotext Geomembr* 29(3):313–322
- Indraratna B, Ngo NT, Rujikiatkamjorn C (2013) Deformation of coal fouled ballast stabilized with geogrid under cyclic load. *J Geotech Geoenviron Eng* 139(8):1275–1289
- Indraratna B, Nimbalkar S, Christie D, Rujikiatkamjorn C, Vinod JS (2010) Field assessment of the performance of a ballasted rail track with and without geosynthetics. *J Geotech Geoenviron Eng ASCE* 136(7):907–917
- Indraratna B, Nimbalkar S (2013) Stress-strain degradation response of railway ballast stabilized with geosynthetics. *J Geotech Geoenviron Eng* 139(5):684–700
- Indraratna B, Nimbalkar S, Neville T (2014a) Performance assessment of reinforced ballasted rail track. In: *Proceedings of the ICE—ground improvement, vol 167, pp 24–34*
- Indraratna B, Ngo NT, Rujikiatkamjorn C, Vinod J (2014b) Behaviour of fresh and fouled railway ballast subjected to direct shear testing—a discrete element simulation. *Int J Geomech ASCE* 14(1):34–44
- Indraratna B, Sun Q, Ngo NT, Rujikiatkamjorn C (2017a) Current research into ballasted rail tracks: model tests and their practical implications. *Aust J Struct Eng*, 1–17
- Indraratna B, Nimbalkar S, Ngo NT, Neville T (2016) Performance improvement of rail track substructure using artificial inclusions—experimental and numerical studies. *Transp Geotech* 8:69–85
- Indraratna B, Sun Q, Grant J (2017b) Behaviour of subballast reinforced with used tyre and potential application in rail tracks. *Transp Geotech* 12:26–36
- Indraratna B, Ngo NT, Rujikiatkamjorn C (2017c) Improved performance of ballasted rail tracks using plastics and rubber inclusions. *Procedia Eng* 189:207–214
- Indraratna B, Sun Q, Heitor A, Grant J (2018) Performance of a rubber tyre-confined capping layer under cyclic loading for railroad conditions. *J Mater Civ Eng ASCE* 30(3):06017021
- Lackenby J, Indraratna B, McDowell GR, Christie D (2007) Effect of confining pressure on ballast degradation and deformation under cyclic triaxial loading. *Géotechnique* 57(6):527–536
- LePen L (2008) *Track behaviour: the importance of the sleeper to ballast interface*. Ph.D. Thesis, University of Southampton, UK
- Li D, Selig ET (1998) Method for railroad track foundation design. I: Development. *J Geotech Geoenviron Eng* 124(4):316–322
- McDowell GR, Harireche O, Konietzky H, Brown SF, Thom NH (2006) Discrete element modelling of geogrid-reinforced aggregates. In: *Proceedings of the ICE—Geotechnical Engineering, vol 159, Issue 1, pp 35–48*
- Ngo NT, Indraratna B, Rujikiatkamjorn C (2014) DEM simulation of the behaviour of geogrid stabilised ballast fouled with coal. *Comput Geotech* 55:224–231

- Ngo T, Indraratna, Rujikiatkamjorn C (2016a) Modelling geogrid-reinforced railway ballast using the discrete element method. *Transp Geotech* 8:86–102
- Ngo NT, Indraratna B, Rujikiatkamjorn C (2017a) A study of the geogrid–subballast interface via experimental evaluation and discrete element modelling. *Granular Matter* 19(3):54–70
- Ngo NT, Indraratna B, Rujikiatkamjorn C (2017b) Stabilisation of track substructure with geoinclusions—experimental evidence and DEM simulation. *Int J Rail Transp* 5(2):63–86
- Ngo NT, Indraratna B, Rujikiatkamjorn C, Biabani MM (2016b) Experimental and discrete element modeling of geocell-stabilised subballast subjected to cyclic loading. *J Geotech Geoenviron Eng* 142(4):04015100
- Nimbalkar S, Indraratna B (2016) Improved performance of ballasted rail track using geosynthetics and rubber shockmat. *J Geotech Geoenviron Eng* 142(8):04016031
- Powrie W, Yang LA, Clayton CRI (2007) Stress changes in the ground below ballasted railway track during train passage. In: *Proceedings of the Institution of Mechanical Engineers, Part F: Journal of Rail and Rapid Transit*, pp 247–261
- Rujikiatkamjorn C, Indraratna B, Ngo NT, Coop M (2012) A laboratory study of railway ballast behaviour under various fouling degree. In: *The 5th Asian regional conference on geosynthetics*, pp 507–514
- Rujikiatkamjorn C, Ngo NT, Indraratna B, Vinod JS, Coop M (2013) Simulation of fresh and fouled ballast behaviour using discrete element method. In: *International Conference on Ground Improvement & Ground Control (ICGI 2012)*, pp 1585–1591
- Selig ET, Waters JM (1994) *Track geotechnology and substructure management*. Thomas Telford, London
- Sun Q, Indraratna B, Nimbalkar S (2016) Deformation and degradation mechanisms of railway ballast under high frequency cyclic loading. *J Geotech Geoenviron Eng* 142(1):04015056
- Sun Q, Indraratna N (2014) Effect of cyclic loading frequency on the permanent deformation and degradation of railway ballast. *Géotechnique* 64(9):746–751
- Tennakoon N, Indraratna B, Rujikiatkamjorn C, Nimbalkar S, Neville T (2012) The role of ballast-fouling characteristics on the drainage capacity of rail substructure. *Geotech Test J* 35(4):1–11
- Trani LD, Indraratna B (2010) Assessment of subballast filtration under cyclic loading. *J Geotech Geoenviron Eng* 136(11):1519–1528
- Tutumluer, Dombrow (2008) *Laboratory characterization of coal dust fouled ballast behaviour*. In: AREMA 2008 annual conference & exposition. Salt Lake City, UT, USA
- Tutumluer E, Huang H, Bian X (2012) Geogrid-aggregate interlock mechanism investigated through aggregate imaging-based discrete element modeling approach. *Int J Geomech* 12(4):391–398